Computer Assisted Mechanics and Engineering Sciences, **3**: 55–64, 1996.

An improved viscous boundary for dynamic soil-structure interaction[1]

Harry A. Dieterman
Delft University of Technology, Faculty of Civil Engineering, Section Applied Mechanics, Stevinweg 1, 2628 CN Delft, The Netherlands

R. Robert Gajewski
Warsaw University of Technology, Faculty of Civil Engineering, Center of Computer Methods, Armii Ludowej 16, 00-637 Warszawa, Poland

(Received August 7, 1995)

In many engineering problems modelling of wave propagation in infinite or semi-infinite domains is of great importance. One of the main limitations of the usage of the finite element method in dynamic soil-structure interaction arises when it is used for the modelling of an infinite domain. If nothing is done to take care of artificial reflections at the mesh boundaries, errors are introduced into the results. To handle the reflections different artificial boundaries have been proposed in the literature and used. This paper deals with an improvement of one of the most widely used local absorbing boundary condition — the standard viscous boundary. Both analytical investigations of the efficiency of the boundary as well as numerical results are presented.

FOREWORD

How to formulate the radiation condition of the unbounded soil is the key issue in the analysis of soil-structure interaction. A real challenge exists to develop a transmitting boundary of higher accuracy which is local in time and space and which can handle (approximately) all types of waves without restrictions to the geometry and on the material properties such as Poisson's ratio. This is definitively the area of soil-structure interaction analysis where the research efforts should be concentrated. [11]

1. INTRODUCTION

In many engineering problems like problems involving transport structures, railways, road tunnels, subways, underground passages in towns, live-line systems, pile-driving, nuclear plants and underground or surface mining of mineral resources the modelling of wave propagation in infinite or semi-infinite domains is of great importance. This paper deals with a brief survey of existing local absorbing boundary conditions. Then an improved viscous boundary is studied for dynamic problems. The last part of the paper deals with the verification of the behaviour of the developed boundary in dynamic problems.

The fundamental objective of the dynamic analysis of a structure-foundation system using finite elements is depicted in Fig. 1. A specified time-varying load acts on the structure. The dynamic response of the structure and, to a lesser extent, of the foundation has to be calculated taking into

[1]The paper was presented at the 12th Polish Conference on Computer Methods in Mechanics in Warsaw–Zegrze on May 9–13, 1995. Further papers presented at the Conference will be published in the forthcoming issues of this Journal.

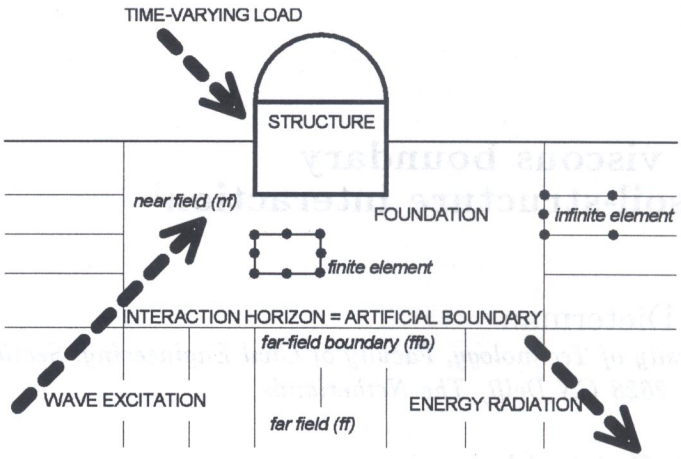

Fig. 1. Discretized model of soil-structure system

account the radiation of energy of the waves propagating into and out of the foundation region not included in the model.

Such interaction problems can be classified into two types according to the source of the dynamic load. One type of the problems involves loads that can be included in the finite element model, such as unbalanced masses in rotating machinery, wind loads, aeroplane impact or an explosion in the surrounding atmosphere. In the other type of problems loading is generated in the foundation medium, such as an earthquake or an underground explosion and results in elastic waves entering into the computational domain.

2. TRANSMITTING BOUNDARIES

One of the limitations of the usage of the finite element method arises when it is used for the modelling of an infinite domain. In dynamic problems energy then radiates from the source outwardly towards infinity. If nothing is done to prevent from artificial reflections at the mesh boundary errors are introduced into the results. To handle reflections several different artificial boundaries have been proposed in the literature and used. The aim of such boundaries is to make them behave as nearly as possible as if the mesh extends to infinity. In literature they are known as transmitting, absorbing or silent boundaries.

Three classes of transmitting boundaries for the numerical analysis of problems of wave propagation in continua of infinite extent are distinguished in literature (see e.g. [8]):

- the elementary (non-transmitting) b.c. which are perfect reflectors,
- the consistent (non-local, perfect transmitting) b.c. which are perfect absorbers,
- the local (imperfect transmitting) b.c. which result in spurious reflections.

Elementary boundary conditions are perfect reflectors. In this case either the displacements or the stresses are prescribed to be zero at the boundary. These boundaries are perfect reflectors in the sense that no energy is absorbed or transmitted. They can only be used if they are placed at sufficiently large distance from the source and when the damping in the modelled material is sufficient.

Consistent boundary conditions are perfectly absorbing boundary conditions for any kind of waves impinging on the boundary with arbitrary incidence. However their realisation requires conditions which are essentially non-local in nature. All degrees of freedom on the boundary are coupled. It destroys the banded structure of the stiffness matrix in a finite element formulation and increases computational cost.

2.1. Local absorbing boundary conditions

Local absorbing boundary conditions (*labc*) are mainly based on physical or mathematical approximations or even on heuristic concepts. As *labc* are approximations of perfectly absorbing conditions full wave absorption can only be obtained for one particular angle of incidence so far. They are usually tailored to perfectly absorb incident waves normal to the boundary, however for non-normal incidence non-perfect absorption results. During the past twenty years many such boundaries were proposed (see [1, 9, 10]). The most of the well-known and commonly used *labc* are mathematically equivalent and therefore they should have comparable wave-absorbing attributes (see [7]).

The first *labc* was formulated by Lysmer and Kuhlemeyer [9]. It was based on the simple physical observation that for plane waves in 1-D and 3-D problems the stresses are proportional to velocities. They used viscous damping forces acting along the free boundary as a means of absorbing the radiated energy which can also be modelled as a set of viscous dashpots (dampers) or damping elements normal and tangential to the boundary. The method is relatively easy to implement. It treats both dilatational and shear waves. The big advantage of viscous dampers is the fact that they are frequency independent. The technique is thus suitable for transient analysis however cannot carry static load. This boundary is also known as the standard viscous boundary (*svb*) or the full-space boundary condition (see [6]).

2.1.1. Standard viscous boundary

Such dampers work perfect if a plane wave travels perpendicular towards the boundary. If the artificial boundary is truncated at a certain but large distance away then the outgoing waves at each point on the introduced convex boundary can be treated as plane waves. The model corresponds to the physical situation in which the truncated boundary is supported on infinitesimal dashpots oriented in normal and tangential directions at the boundary.

The basic idea of the boundary proposed by Lysmer and Kuhlemeyer is illustrated in Fig. 2 for the plane strain case. One applies boundary stresses σ and τ to an otherwise free boundary to cancel the stresses which are produced at the boundary by the incoming waves. It can be written as equations of zero-traction condition at the free boundary

$$\begin{aligned} (\sigma_{\text{in}} + \sigma_{\text{bd}}) + \sigma_{\text{rf}} &= 0\,, \\ (\tau_{\text{in}} + \tau_{\text{bd}}) + \tau_{\text{rf}} &= 0 \end{aligned} \tag{1}$$

in which 'in' stands for incident stresses, 'bd' for applied boundary stresses and 'rf' for reflected wave stresses.

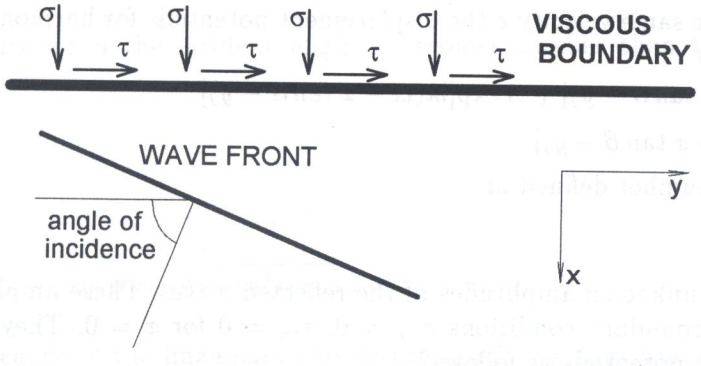

Fig. 2. Orientation of wave and schematic representation of a viscous boundary

The effect of the exterior region on the interior region is identical to that of an energy absorbing or non-reflecting boundary. This observation leads directly to the idea of determining the dynamic response of the interior region from a finite model consisting of the interior region subjected to a

boundary condition which ensures that all energy arriving at the boundary is absorbed. Lysmer and Kuhlemeyer [9] have investigated different possibilities for expressing this boundary condition analytically and have found the most promising way to express it by the following conditions

$$\begin{aligned} \sigma_{xx} &= a\rho c_{\mathrm{p}}\dot{u}\,, \\ \tau_{xy} &= b\rho c_{\mathrm{s}}\dot{v} \end{aligned} \tag{2}$$

where ρ is the mass density, c_{p} and c_{s} are the pressure and shear wave velocities respectively, a and b are dimensionless parameters.

The proposed boundary condition corresponds to a situation in which the convex boundary is supported on infinitesimal dashpots oriented normal and tangential to the boundary. The efficiency of the boundary will be studied in a similar way as it was done in [9] and [10].

3. Boundary reflections

The situation studied in the case of an incident P-wave is shown in Fig. 3. The y-axis represents the viscous boundary and the elastic medium is located in the lower half plane. The incident wave generates two reflected waves.

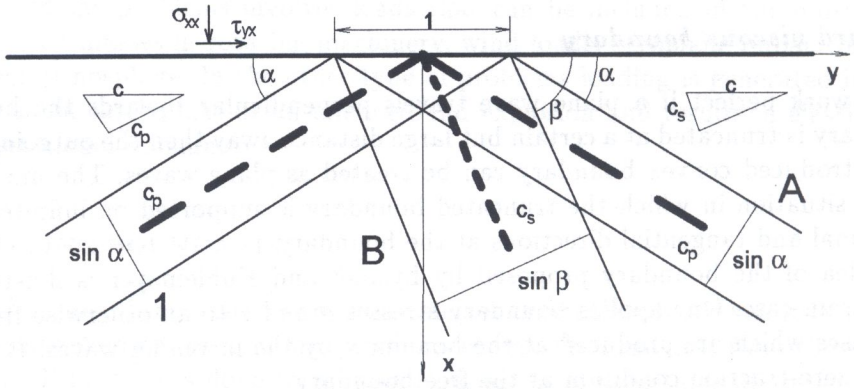

Fig. 3. Incident P-wave at the boundary

The horizontal and vertical displacements may be written in terms of the displacement potentials Φ and Ψ (in usual form) in which Φ is related to the displacements due to the P-waves and Ψ to the S-waves respectively.

Since the wave fronts of three waves (incident P-wave and reflected P- and S-waves) must travel along the y-axis at the same velocity c the displacement potentials for harmonic waves of frequency ω must have the form

$$\begin{aligned} \Phi &= \exp[\mathrm{i}k(ct + x\tan\alpha - y)] + A\exp[\mathrm{i}k(ct - x\tan\alpha - y)] \\ \Psi &= B\exp[\mathrm{i}k(ct - x\tan\beta - y)] \end{aligned} \tag{3}$$

where k is the wave number defined as

$$k = \frac{\omega}{c} \tag{4}$$

and A and B are the unknown amplitudes of the reflected waves. These amplitudes may be determined by the stress boundary conditions $\sigma_{xx} = 0$, $\tau_{xy} = 0$ for $x = 0$. They can be expressed in terms of displacement potentials as follows

$$\begin{aligned} &\frac{1-2\kappa^2}{\kappa^2}\nabla^2\Phi + 2\left(\frac{\partial^2\Phi}{\partial x^2} + \frac{\partial^2\Psi}{\partial x\partial y}\right) = \frac{a}{\kappa c_{\mathrm{s}}}\left(\frac{\partial\dot{\Phi}}{\partial x} + \frac{\partial\dot{\Psi}}{\partial y}\right), \\ &2\frac{\partial^2\Phi}{\partial x\partial y} + \frac{\partial^2\Psi}{\partial y^2} - \frac{\partial^2\Psi}{\partial x^2} = \frac{b}{c_{\mathrm{s}}}\left(\frac{\partial\dot{\Phi}}{\partial y} + \frac{\partial\dot{\Psi}}{\partial x}\right), \end{aligned} \tag{5}$$

where κ can be defined according to Snell's law as

$$\kappa = \frac{c_s}{c_p} = \sqrt{\frac{1-2\nu}{2(1-\nu)}}\,. \tag{6}$$

Substituting Eqs. $(3)_{1,2}$ into $(5)_{1,2}$ results in two linear equations

$$\begin{aligned}(1-2\kappa^2\cos\alpha + a\sin\alpha)A + (\sin 2\beta + a\cos\alpha)B &= 2\kappa^2\cos^2\alpha - 1 + a\sin\alpha\,,\\ (\kappa^2\sin 2\alpha + b\cos\beta)A + (\cos 2\beta - b\sin\beta)B &= \kappa^2\sin 2\alpha - b\cos\beta\,,\end{aligned} \tag{7}$$

from which the amplitudes A and B may be obtained as functions of the incident angle.

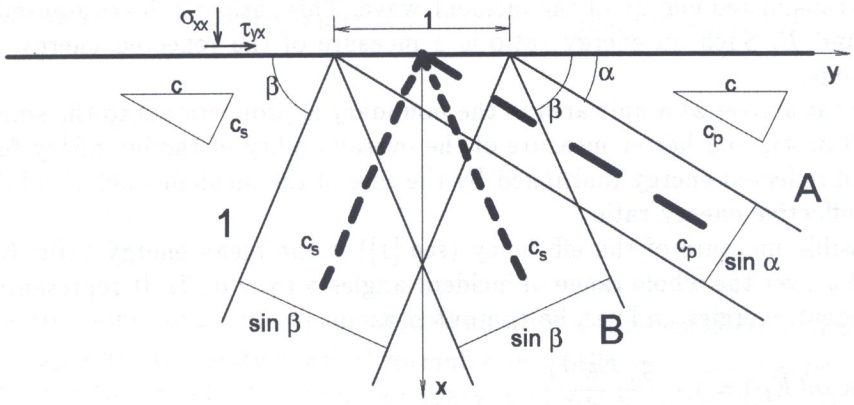

Fig. 4. Incident S-wave at the boundary

The incident S-wave case shown in Fig. 4 can be studied in a similar way as the P-wave case. The expressions for the displacement potentials should be replaced by

$$\begin{aligned}\Phi &= A\exp[ik(ct - x\tan\alpha - y)]\,,\\ \Psi &= \exp[ik(ct + x\tan\beta - y)] + B\exp[ik(ct - x\tan\beta - y)]\,.\end{aligned} \tag{8}$$

The linear equations used to define A and B are in this case

$$\begin{aligned}(\kappa^2\sin 2\alpha + b\cos\beta)A + (\cos 2\beta - b\sin\beta)B &= -\cos 2\beta - b\sin\beta\,,\\ (-\cos 2\beta + a\sin\alpha)A + (\sin 2\beta + a\cos\alpha)B &= \sin 2\beta - a\cos\alpha\,.\end{aligned} \tag{9}$$

A special case occurs when the incident angle β becomes smaller than the critical angle β^* defined by

$$\cos\beta^* = \kappa\,. \tag{10}$$

In that case we have

$$\cos\alpha = \frac{\cos\beta}{\kappa} > 1\,, \qquad \sin\alpha = -\mathrm{i}\sqrt{\cos^2\alpha - 1}\,. \tag{11}$$

The physical significance of the imaginary sine of the angle α is that the appropriate reflected P-wave does not exist but instead a surface wave shows up, travelling along the boundary and not back into the continuum. Coefficients of equations $(9)_{1,2}$ now become complex, and so are the amplitudes $A = A_1 + \mathrm{i}A_2$ and $B = B_1 + \mathrm{i}B_2$. The amplitude of the boundary wave decreases with distance from the boundary and does not reflect energy back into the continuum, thus it gives no contribution to the reflected energy.

4. Efficiency considerations

The energy transmitted per unit of time (power) through a unit area of the wave front of an S-wave with amplitude B is

$$E_s = \frac{1}{2}\rho\, c_s \omega^2 B^2. \tag{12}$$

The similar expression for a P-wave of amplitude A is

$$E_p = \frac{1}{2}\rho \frac{c_s}{\kappa} \omega^2 A^2. \tag{13}$$

A good measure of the ability of the standard viscous boundary to absorb impinging elastic waves is the energy ratio E_R defined as the ratio between the transmitted energy of the reflected waves and the transmitted energy of the incident wave. This ratio can be computed from the wave amplitudes A and B. Such an energy ratio is a measure of the reflected energy for a particular incident angle only.

The energy that arrives at a unit area of the boundary is proportional to the sine of the incident wave (see Fig. 3 or 4), so a better measure of the overall ability of the boundary to absorb energy is the product of reflected energy multiplied by the sine of the incident angle, and denoted by E_E. It is called the effective energy ratio.

Another possible measure of the efficiency (see [1]) is the mean energy ratio E_M which is the mean value of E_E over the whole range of incident angles γ ($\gamma = \alpha, \beta$). It represents the average of reflected to incident energies and can be computed as

$$E_M = 1 - \text{mean}(E_E) = 1 - \frac{\int_\gamma E_E \, d\gamma}{\int_\gamma d\gamma}. \tag{14}$$

Figure 5 depicts the variation of the effective energy ratio E_E for a P-wave with the angle α for different values of ν. The worst behaviour of the boundary is observed for small angles. It further shows that the absorbing capabilities of the boundary are decreasing for higher values of ν.

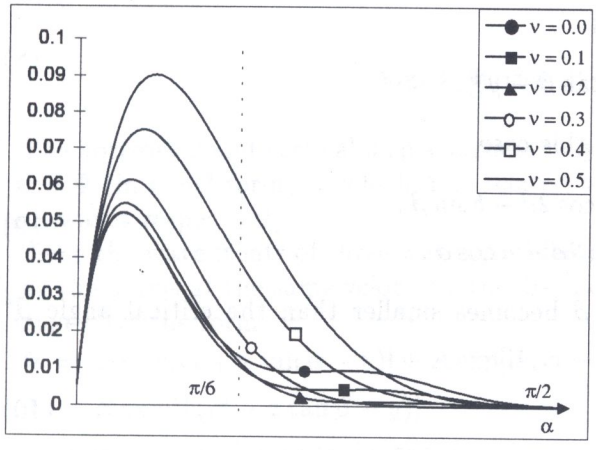

Fig. 5. Effective energy ratio E_E for incident P-waves

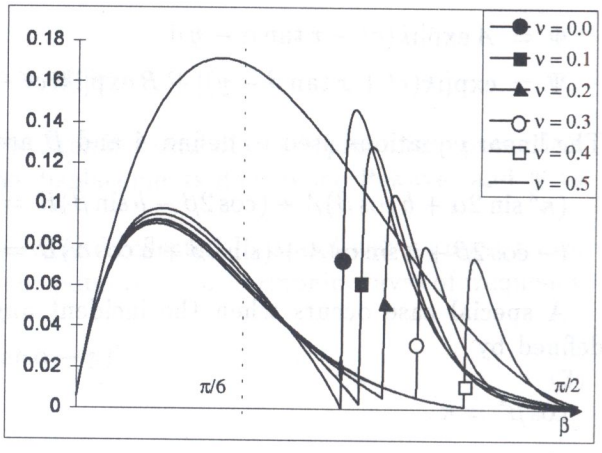

Fig. 6. Effective energy ratio E_E for incident S-waves

In the case of an incident S-wave for the region where the incident wave angle β is smaller than critical β^*, the boundary wave does not reflect energy back into the continuum and it makes no contribution to the energy ratio.

Figure 6 shows the effective energy ratio E_E for a S-wave as function of the angle β for different values of Poisson's ratio. Large differences in absorbing properties are observed near the critical angle which is located in the range $[\pi/4, \pi/2]$. Different from the incident P-wave case the absorbing properties of the boundary for $\nu < 0.4$ and $\beta < \beta^*$ are nearly identical. For ν in the range [0.4, 0.5] the effective energy ratio increases substantially.

5. IMPROVED VISCOUS BOUNDARY

Improved viscous boundary (*ivb*) conditions have been described in detail in [5] and presented in [3, 4]. They have a term to account for the non-plane wave fronts. The *ivb* conditions are obtained by expressing the normal derivatives of the displacements in terms of the velocities

$$\begin{aligned} \frac{\partial u}{\partial x} &= \frac{1}{c_{\mathrm{p}}}\dot{u}\,, \\ \frac{\partial v}{\partial x} &= \frac{1}{c_{\mathrm{s}}}\dot{v} \end{aligned} \tag{15}$$

and then substituting them into the expressions for the boundary stresses. It results in the following equations

$$\begin{aligned} \sigma_{xx} &= \rho c_{\mathrm{p}}\dot{u} + \left[\lambda\frac{\partial v}{\partial y}\right]\gamma_1\,, \\ \tau_{xy} &= \rho c_{\mathrm{s}}\dot{v} + \left[\mu\frac{\partial u}{\partial y}\right]\gamma_2\,, \end{aligned} \tag{16}$$

where μ and λ are Lame constants, γ_1 and γ_2 are additional dimensionless multipliers.

Equations $(16)_{1,2}$ are the mathematical formulation of the improved viscous boundary conditions. They include the standard viscous boundary as a special case ($\gamma_1 = \gamma_2 = 0$), i.e. for the plane wave case. The second term on the right hand side of Eq. $(16)_{1,2}$ will be zero if the waves are purely plane. It is reasonable to expect, that such a modified viscous boundary will perform better in practical computations where waves generally do not propagate in a plane wave form.

The efficiency of the *ivb* has been investigated in a similar way as for the *svb*. The best relative improvements in the energy ratio with respect to the *svb* obtained for $\gamma_1 = \gamma_2 = 1$, $a = b = 1$ and for incident angles of P- and S-waves smaller than $\pi/6$ are presented in Fig. 7.

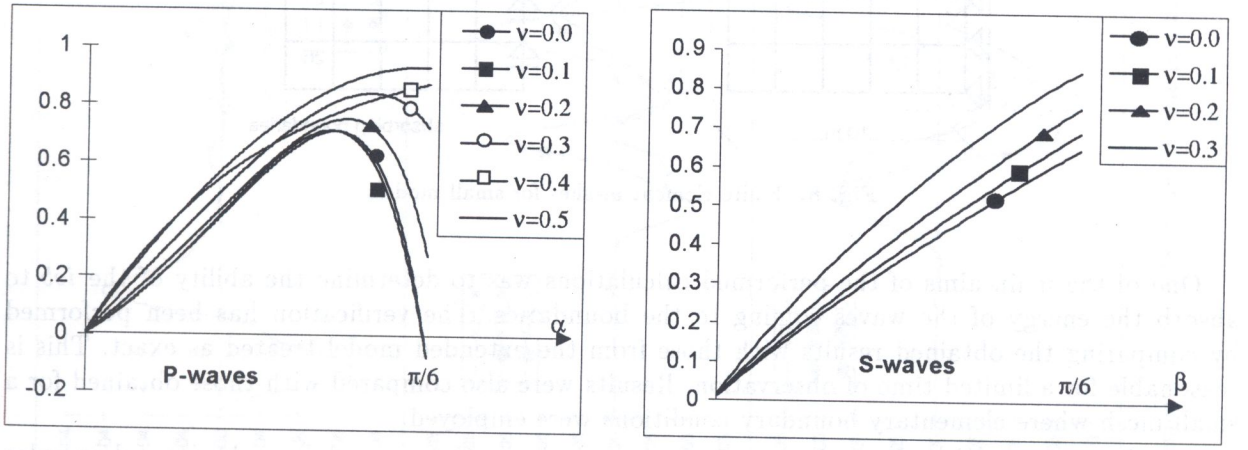

Fig. 7. Relative improvements of the energy ratio E_R

The figure shows the differences in the relative improvements of the energy ratio E_R obtained for various values of the Poisson's ratio. Relative improvements for an incident P-wave are larger for higher values of ν. The maximum relative improvement of E_R is 90% in the range up to $\pi/6$.

Similar results are obtained for an incident S-wave. For $\nu > 0.3$ no improvement was observed. For $\nu < 0.3$ the maximum relative improvement is also up to 90%.

6. Implementation and numerical results

The *ivb* has been implemented into the finite element code DIANA in a similar way as the *svb*. For a two-noded element with length l the stiffness and damping matrices have the following forms

$$K_t = \begin{bmatrix} 0 & -\frac{1}{2}\lambda & 0 & \frac{1}{2}\lambda \\ -\frac{1}{2}\mu & 0 & \frac{1}{2}\mu & 0 \\ 0 & -\frac{1}{2}\lambda & 0 & \frac{1}{2}\lambda \\ -\frac{1}{2}\mu & 0 & \frac{1}{2}\mu & 0 \end{bmatrix}, \qquad C_t = \begin{bmatrix} 2c_1 & 0 & c_1 & 0 \\ 0 & 2c_2 & 0 & c_2 \\ c_1 & 0 & 2c_1 & 0 \\ 0 & c_2 & 0 & 2c_2 \end{bmatrix}, \tag{17}$$

where $c_1 = \rho c_p l/6$, $c_2 = \rho c_s l/6$.

The meshes used for numerical tests were definitely coarser than those normally used for practical engineering problems. The purpose of the tests was to evaluate and compare results obtained for a small model without and with *ivb* to those obtained from an extended model, large enough to avoid spurious reflections.

All of the loading was applied on one node and only for a few time-steps. This input, similar to a delta function, contains high-frequencies. This approach was selected since it subjects the viscous boundaries to relatively severe conditions. The two kinds of excitations which were considered are a vertical pulse that generates mainly dilatational waves and a horizontal pulse that generates primarily shear waves. They were applied at the top surface in the left upper corner (see Fig. 8). These loadings were selected because of their simplicity and their relevance to the vertical and horizontal loadings that occur in dynamic soil-structure interaction (see [2]).

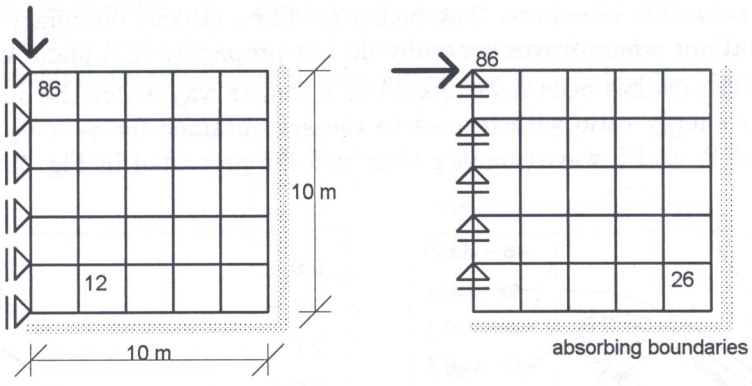

Fig. 8. Finite element meshes for small models

One of the main aims of the performed calculations was to determine the ability of the *ivb* to absorb the energy of the waves coming to the boundaries. The verification has been performed by comparing the obtained results with those from the extended model treated as exact. This is reasonable for a limited time of observation. Results were also compared with those obtained for a small mesh where elementary boundary conditions were employed.

The first presented example concerns the wave propagation caused by a horizontal impulse applied to a half-space. Horizontal and vertical displacements of selected points of the mesh are depicted in Fig. 9. In all figures results for the extended mesh, for the small mesh with elementary boundary conditions and for the mesh with the *ivb* are denoted by e, s and i, respectively.

The second example concerns the wave propagation due to a vertical impulse. Displacements of selected points are depicted in Fig. 10.

All pictures show the ability of the improved viscous boundary to model infinite media (elastic half-space).

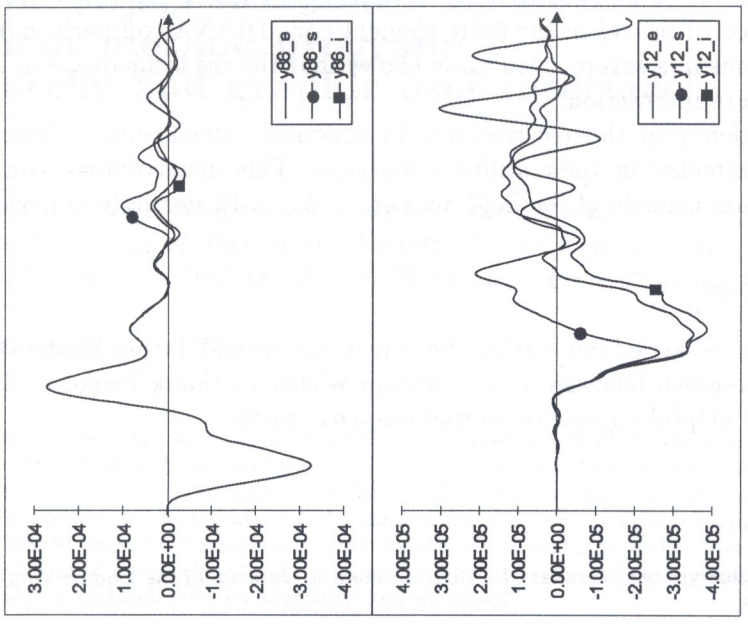

Fig. 10. Displacements of the nodes 86 and 12 due to a vertical pulse

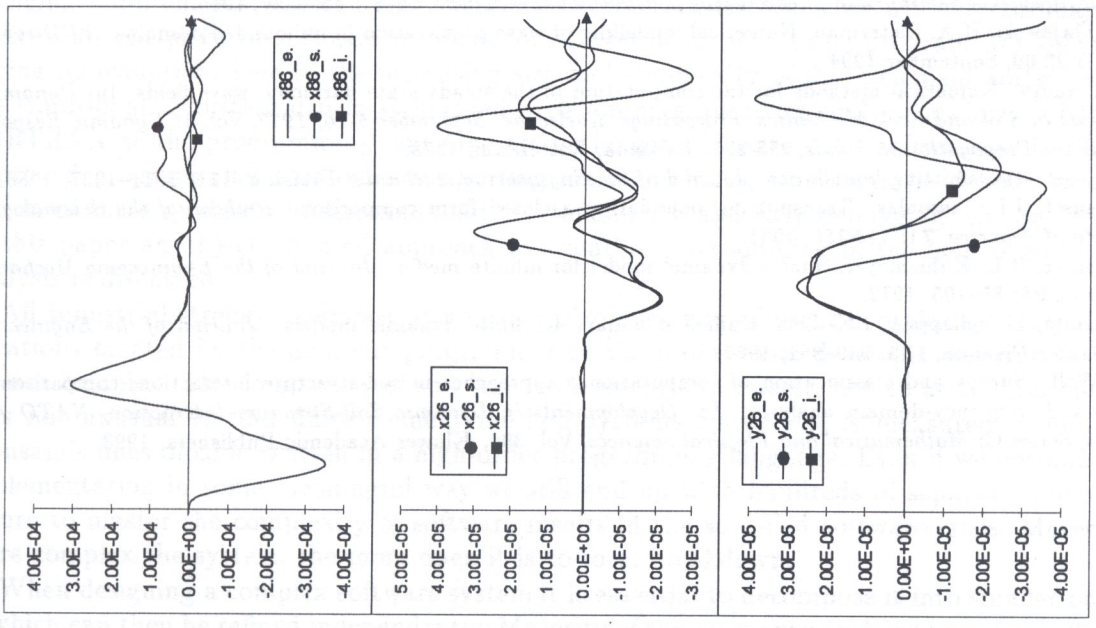

Fig. 9. Displacements of the nodes 86 and 26 due to a horizontal pulse

7. Conclusions

In this paper the standard viscous boundary (*svb*) has been improved by accounting for the non-planarity of the wavefronts. The ability of the improved viscous boundary (*ivb*) to absorb the incoming energy shows to be substantially better.

After implementation of the *ivb* in the finite element code DIANA comparison of its performance with an "exact" solutions in a severe calculation shows that the *ivb* is adequate in modelling infinite domains in soil-structure interaction.

The numerical efficiency of the *ivb* elements in practical calculations is lower than expected, due to the lack of symmetry in their stiffness matrices. This disadvantage can be overcome by developing a subprogram capable of solving linear equations with partially nonsymmetric matrices.

Acknowledgement

These investigations were carried out during the stay of the second author at the Delft University of Technology during a research fellowship. This author wishes to thank Professor J. Blaauwendraad for his inspiration and helpful comments during one year work.

References

[1] T. Akiyoshi. Compatible viscous boundary for discrete models. *Journal of the Engineering Mechanics Division*, **104**: 1253–1266, 1978.

[2] M. Cohen, P.C. Jennings. Silent boundary methods for transient analysis. In: *Mechanics and Mathematical Methods — Computational Methods in Mechanics*, Computational Methods for Transient Analysis, 301–360. North-Holland, Amsterdam, 1983.

[3] H. Dieterman, R. Gajewski. An improved viscous boundary in numerical modelling of wave propagation in unbounded domains. In: *Computer Methods in Mechanics, Proceedings of the XII Polish Conference on CMM*, 86–87. Military University of Technology, Warsaw, 1995.

[4] R.R. Gajewski. Local absorbing boundary conditions in the dynamic soil-structure interaction. In: *IV Polsko-Rosyjskie Seminarium "Teoretyczne podstawy budownictwa"*, 75–87. Moscow, 1995.

[5] R.R. Gajewski, H.A. Dieterman. Numerical modelling of wave propagation in unbounded domains. *TUD-report*, 03.21.1.22.09, September 1994.

[6] W.A. Haupt. Numerical methods for the computation of the steady-state harmonic wave fields. In: *Dynamical Methods in Soil and Rock Mechanics, Proceedings, Karlsruhe, September 5-16, 1977*, Vol. 1: *Dynamic Response and Wave Propagation in Solids*, 255-280. Balkema, Rotterdam, 1978.

[7] E. Kausel. Transmitting boundaries. *Journal of the Engineering Mechanics Division*, **114**: 1011–1027, 1988.

[8] E. Kausel, J.L. Tassoulas. Transmitting boundaries: a closed form comparison. *Bulletin of the Seismological Society of America*, **71**: 143-159, 1981.

[9] J. Lysmer, R.L. Kuhlemeyer. Finite dynamic model for infinite media. *Journal of the Engineering Mechanics Division*, **95**: 85–105, 1972.

[10] W. White, S. Valiappan, I.K. Lee. Unified boundary for finite dynamic models. *Journal of the Engineering Mechanics Division*, **103**: 949–964, 1977.

[11] J.P. Wolf. Survey and classification of computational approaches in soil-structure interaction: comparison of time- and frequency-domain analyses, In: *Developments in Dynamic Soil-Structure Interaction, NATO ASI Series*, Series C: *Mathematical and Physical Sciences*, Vol. 390. Kluwer Academic Publishers, 1993.